frontiers | Frontiers in Neurology

TYPE Original Research
PUBLISHED 24 January 2023
DOI 10.3389/fneur.2022.979659

OPEN ACCESS

EDITED BY
Ingo Kleiter,
Marianne-Strauss-Klinik, Germany

REVIEWED BY
Simon Faissner,
St. Josef-Hospital, Germany
Andreia Barateiro,
Research Institute for Medicines (iMed.ULisboa), Portugal

*CORRESPONDENCE
Michael Davin Kornberg
✉ michael.kornberg@jhmi.edu

SPECIALTY SECTION
This article was submitted to Multiple Sclerosis and Neuroimmunology, a section of the journal Frontiers in Neurology

RECEIVED 27 June 2022
ACCEPTED 30 December 2022
PUBLISHED 24 January 2023

CITATION
Godfrey WH, Hwang S, Cho K, Shanmukha S, Gharibani P, Abramson E and Kornberg MD (2023) Therapeutic potential of blocking GAPDH nitrosylation with CGP3466b in experimental autoimmune encephalomyelitis. *Front. Neurol.* 13:979659. doi: 10.3389/fneur.2022.979659

Therapeutic potential of blocking GAPDH nitrosylation with CGP3466b in experimental autoimmune encephalomyelitis

Wesley H. Godfrey[1], Soonmyung Hwang[1], Kaho Cho[1], Shruthi Shanmukha[2], Payam Gharibani[1], Efrat Abramson[1] and Michael Davin Kornberg[1]*

[1]Department of Neurology, Johns Hopkins School of Medicine, Baltimore, MD, United States, [2]Department of Psychiatry and Behavioral Sciences, Johns Hopkins School of Medicine, Baltimore, MD, United States

Multiple sclerosis (MS) is a neuroinflammatory disease of the central nervous system (CNS). Although classically considered a demyelinating disease, neuroaxonal injury occurs in both the acute and chronic phases and represents a pathologic substrate of disability not targeted by current therapies. Nitric oxide (NO) generated by CNS macrophages and microglia contributes to neuroaxonal injury in all phases of MS, but candidate therapies that prevent NO-mediated injury have not been identified. Here, we demonstrate that the multifunctional protein glyceraldehyde-3-phosphate dehydrogenase (GAPDH) is robustly nitrosylated in the CNS in the experimental autoimmune encephalomyelitis (EAE) mouse model of MS. GAPDH nitrosylation is blocked *in vivo* with daily administration of CGP3466b, a CNS-penetrant compound with an established safety profile in humans. Consistent with the known role of nitrosylated GAPDH (SNO-GAPDH) in neuronal cell death, blockade of SNO-GAPDH with CGP3466b attenuates neurologic disability and reduces axonal injury in EAE independent of effects on the immune system. Our findings suggest that SNO-GAPDH contributes to neuroaxonal injury during neuroinflammation and identify CGP3466b as a candidate neuroprotective therapy in MS.

KEYWORDS

nitric oxide, multiple sclerosis, GAPDH, nitrosylation, neuroprotection, neuroinflammation, experimental autoimmune encephalomyelitis

1. Introduction

Multiple sclerosis (MS) is an autoimmune disease of the central nervous system (CNS) that affects nearly 1 million people in the United States (1). MS is classically characterized by inflammatory attack against oligodendrocytes, which are the myelin-producing cells crucial for efficient transduction of action potentials along axons, leading to demyelination. The disease is further characterized by gliosis and neurodegeneration (2). The two main types of MS are relapsing-remitting MS (RRMS), which is characterized by discrete neurologic "relapses" associated with focal inflammatory attack within the CNS, and progressive MS defined by insidious disability progression in the absence of relapse. Despite a historical focus on demyelination, neuroaxonal loss occurs in all phases of MS and represents a primary source of neurologic disability (3), with distinct but overlapping immune mechanisms producing injury in RRMS vs. progressive MS (4–8). Currently approved therapies target the peripheral immune system to limit relapses, but none mitigates neuroaxonal injury during relapse or slows the

accelerating neurodegeneration associated with progressive MS (9). Therefore, a significant unmet clinical need exists for neuroprotective therapies that prevent inflammatory neuroaxonal damage.

During inflammation, a variety of free radicals are generated (10). One particularly potent free radical is nitric oxide (NO), a gaseous, highly reactive molecule associated with inflammatory damage (11). The primary source of NO in neuroinflammation is microglia and CNS-resident macrophages, which contribute to neuroaxonal injury in both relapsing and progressive forms of disease (3, 6). NO produced by activated microglia and macrophages plays a key role in MS pathology (7, 8), as it is found in high concentrations within inflammatory MS lesions (12, 13). In experimental autoimmune encephalomyelitis (EAE), the primary mouse model of MS, locally administered NO scavengers prevent axonal degeneration (14), and NO donors replicate EAE-like axonal pathology (15). However, no current therapies target NO-mediated CNS injury.

A primary mode of action of NO signaling is protein S-nitrosylation, a redox-based modification of cysteine residues within target proteins (16, 17). The glycolytic enzyme glyceraldehyde-3-phosphate dehydrogenase (GAPDH) is physiologically nitrosylated at its Cys150 residue, which inactivates its enzyme activity and produces a role in signal transduction mediated by binding to Siah1 and nuclear translocation (18). In the nucleus, nitrosylated GAPDH (SNO-GAPDH) leads to cell death *via* p300/CBP and p53 pathways (18, 19) and trans-nitrosylates nuclear proteins (20), with these studies demonstrating a role in neuronal injury. Furthermore, GAPDH nitrosylation was previously reported in the context of neuroinflammation (21). We therefore wondered whether blocking GADPH nitrosylation might be neuroprotective in the context of neuroinflammatory disease.

CGP3466b (Omigapil) is a CNS-penetrant compound with broad anti-apoptotic properties that is structurally similar to the anti-parkinsonian drug L-deprenyl (selegiline) but without effects on monoamine oxidase (22, 23). Notably, CGP3466b blocks GAPDH nitrosylation without affecting GAPDH enzyme activity, and blockade of GAPDH nitrosylation is crucial for the drug's anti-apoptotic effect (24, 25). CGP3466b showed exceptional promise at eliciting neuroprotection in pre-clinical mouse models of Parkinson's disease (PD) and amyotrophic lateral sclerosis (ALS) but unfortunately failed to meet primary endpoints in clinical trials (26, 27). While nitrosative stress plays a large role in the pre-clinical animal models of these diseases, the factors contributing to the respective human diseases are very complex (28, 29). In contrast, MS pathology in humans is largely driven by inflammation, which is a major source of NO, and there is strong evidence for the involvement of NO in axonal damage in human MS (7, 8, 30). As such, there is a strong biological rationale for exploring CGP366b as a neuroprotective therapy in MS.

No animal model fully captures the complex neurological and immunological milieu found in MS (31). However, in this paper we model key aspects of MS pathology with MOG_{35-55} EAE. This model involves immunizing C57BL/6 mice with a myelin oligodendrocyte glycoprotein (MOG)-derived peptide in combination with complete Freund's adjuvant and pertussis toxin (32), initiating an inflammatory immune response targeting CNS myelin and producing quantifiable neurologic deficits beginning around post-immunization day (PID) 10. In addition to demyelination, MOG_{35-55} EAE is associated with significant neuroaxonal injury which is dependent on NO (14), making it an ideal model in which to study inflammatory neurodegeneration. Importantly, MOG_{35-55} EAE has proven useful in clinical translation, playing a key role in the identification and development of several currently approved MS therapies (33).

In this study, we explore the potential of CGP3466b as a novel therapy for MS. We show that GAPDH is robustly nitrosylated within the CNS during MOG_{35-55} EAE, which is prevented by systemic CGP3466b administration. We further demonstrate that CGP3466b is directly neuroprotective *in vivo*, ameliorating EAE disease severity and reducing neuroaxonal damage in the optic nerve. Finally, we show that CGP3466b acts independently of the peripheral immune system, having minimal effects on immunophenotype *in vitro* and *in vivo*. We conclude that CGP3466b holds promise as an adjunctive neuroprotective therapy in MS.

2. Results

2.1. Neuroinflammation leads to GAPDH nitrosylation within the CNS in the MOG_{35-55} EAE mouse model of MS, which is prevented by CGP3466b treatment

To determine whether SNO-GAPDH might play a role in neuroinflammatory injury, we first examined whether GAPDH nitrosylation occurs within the CNS during the course of MOG_{35-55} EAE. Using the well-described biotin switch assay for detection of nitrosylated proteins (34), we found that GAPDH nitrosylation increased dramatically in spinal cord (the primary site of neuroinflammation in EAE) with a time course that matched the CNS inflammatory response (Figure 1A; Supplementary Figure 1A). SNO-GAPDH levels increased beginning at the onset of neurologic symptoms (PID 10) and reached maximal levels at peak disease (PID 15), representing the peak of neuroinflammation and neurologic disability. Resolution of neuroinflammation (PID 28) was associated with a return of SNO-GAPDH levels to baseline, as macrophage/microglia activation (and resulting NO production) subsided. Together, these results demonstrate that GAPDH nitrosylation is a major consequence of neuroinflammation in a mouse model of MS.

We then sought to determine whether GAPDH nitrosylation in EAE could be prevented with systemic administration of CGP3466b, similar to other experimental models (22, 35). Mice were treated with vehicle or CGP3466b daily *via* intraperitoneal (i.p.) injection beginning on PID 0, and GAPDH nitrosylation was measured by biotin switch assay from spinal cord lysates at PID 15. We found that CGP3466b treatment prevented GAPDH nitrosylation, with maximal effect at 4 mg/kg (Figure 1B; Supplementary Figure 1B). Blockade of nitrosylation was specific to SNO-GAPDH, as CGP3466b had no effect on nitrosylation of β-tubulin.

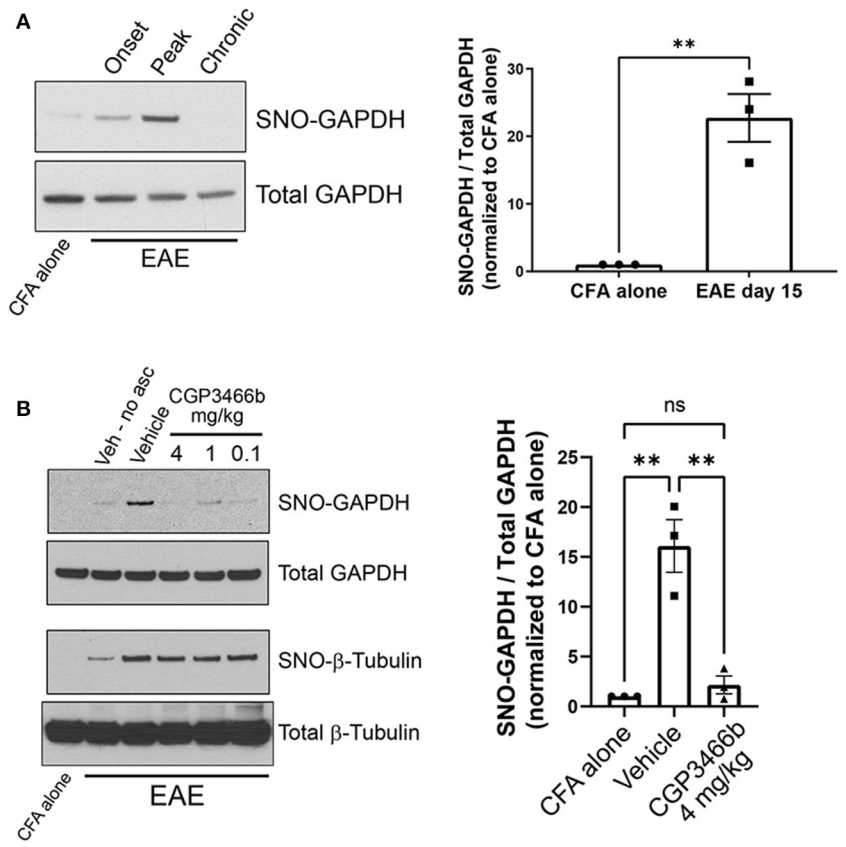

FIGURE 1
CGP3466b prevents GAPDH nitrosylation within the CNS in the MOG_{35-55} EAE mouse model of MS. **(A)** Nitrosylated GAPDH (SNO-GAPDH) was assayed by biotin switch from spinal cord lysates in control (CFA alone) mice at day 15 and at onset (post-immunization day 10), peak (post-immunization day 15), and chronic (post-immunization day 28) stages of EAE. Total GAPDH in tissue lysate was included as loading control. (Left) Representative immunoblot. (*Right*) Quantification of SNO-GAPDH at peak EAE. The ratio of SNO-GAPDH to total GAPDH band intensity was used for quantification, and results were normalized to CFA alone control. Data represent mean ± SEM of three mice per group. **(B)** CGP3466b was administered at indicated doses by daily i.p. injection beginning on post-immunization day 0, and nitrosylated GAPDH and β-tubulin were assayed by biotin switch on post-immunization daiy 15. (*Left*) Representative immunoblot. "No asc" = no ascorbate control. (*Right*) Quantification of SNO-GAPDH levels following treatment with vehicle or CGP3466b 4 mg/kg. SNO-GAPDH levels were quantified as described in **(A)**. Data represent mean ± SEM of three mice per group. $^{**}p < 0.01$ by student's *t*-test **(A)** or one-way ANOVA with Tukey's multiple comparisons test **(B)**. Full blots are shown in Supplementary Figure 1.

2.2. Blocking SNO-GAPDH with CGP3466b is neuroprotective in the EAE model of multiple sclerosis

Given the known role of SNO-GAPDH in neuronal cell injury (18, 19, 36, 37), we examined whether blockade of GAPDH nitrosylation with CGP3466b attenuates neurologic deficits in EAE. To answer this question, we first utilized a prophylactic treatment paradigm, in which mice were randomized to daily treatment with vehicle or CGP3466b beginning on the day of MOG_{35-55} immunization (PID 0). Based on our previous findings, we used the dose of CGP3466b (4 mg/kg) that maximally prevented GAPDH nitrosylation in this model. Mice were clinically scored in a blinded fashion through PID 31. In this treatment paradigm, we found that CGP3466b significantly attenuated the severity of EAE (Figure 2A).

In MOG_{35-55} EAE, the myelin-directed immune response begins in the peripheral immune system, with dendritic cells presenting MOG-derived peptide to CD4 cells in peripheral lymph nodes and spleen. These peripherally activated CD4 cells then infiltrate the CNS and activate local macrophages and microglia to produce demyelination and neuroaxonal injury. This peripheral immune activation determines the onset of neuroinflammation and produces systemic weight loss that precedes neurologic deficits. In the prophylactic treatment paradigm described above, treatment with CGP3466b had no effect on the timing of disease onset or the degree of weight loss (Figure 2B), suggesting that the attenuated neurologic deficits observed with CGP3466b might be due to direct neuroprotection from inflammatory injury rather than peripheral anti-inflammatory effects. To further explore this possibility, we examined the impact of CGP3466b when treatment began on PID 10, a time point subsequent to priming of the peripheral immune response. This paradigm also more closely approximates a therapeutic clinical scenario, in which treatment begins after the onset of disease. We found that daily treatment with CGP3466b beginning on PID 10 similarly attenuated neurologic disability at PID 28 (Figure 2C).

To determine the impact of SNO-GAPDH blockade with CGP3466b on neuroaxonal integrity directly, we examined the optic nerve. The optic nerve is a primary site of neuroinflammation and inflammatory axonal injury in EAE, in analogy to optic neuritis occurring in humans as a consequence of MS (38, 39). Axonal damage can be readily quantified in the optic nerve during EAE

with SMI-32 immunofluorescent staining for non-phosphorylated neurofilament heavy chain, which labels injured axonal spheroids (40). We initiated daily treatment with vehicle or 4 mg/kg CGP3466b on PID 0 in an independent cohort of mice subjected to MOG_{35-55} EAE and quantified SMI-32+ axonal spheroids in the proximal optic nerve on PID 28. CGP3466b-treated mice had fewer SMI-32+ axonal spheroids, indicating reduced axonal injury with CGP3466b treatment (Figure 2D). To determine whether similar neuroprotection could be achieved in a therapeutic paradigm, we initiated treatment on PID 10 and again quantified SMI-32+ axonal spheroids in the proximal optic nerve on PID 28 (Figure 2E). Similar to the prophylactic treatment regimen, CGP3466b-treated mice had significantly fewer SMI-32+ spheroids.

We also examined demyelination in the optic nerves of mice subjected to MOG_{35-55} EAE and treated with vehicle or CGP3466b beginning on PID 0, as measured by immunofluorescence staining for myelin basic protein (MBP) (Supplementary Figure 2, corresponding to the same optic nerves analyzed for SMI-32 staining in Figure 2D). We noted a non-significant trend toward increased MBP staining with CGP3466b treatment, suggesting the intriguing possibility that blockade of SNO-GAPDH produces neuroprotection out of proportion to effects on demyelination. In other words, SNO-GAPDH may play a greater role in axonal compared to oligodendrocyte/myelin injury. This finding is consistent with prior work demonstrating that focal axonal degeneration produced by reactive oxygen and nitrogen species during EAE occurs even in axons with intact myelin sheaths (14).

2.3. CGP3466b has minimal direct effects on myeloid and lymphoid cells *in vitro*

Although the above findings suggest that CGP3466b attenuates neurologic disability in EAE through direct neuroprotection rather than peripheral anti-inflammatory effects, we next asked whether CGP3466b has a quantifiable impact on the activation of cultured immune cells. Beginning with bone marrow derived macrophages (BMMs), we found that CGP3466b had no effect on LPS-stimulated secretion of IL-6, IL-1β, or IL-10 over a range of doses, as measured by enzyme-linked immunosorbent assay (ELISA) (Figure 3A). We then evaluated the effect of CGP3466b on LPS-stimulated expression of the activation markers CD86 and MHC II in BMMs (Figure 3B) and bone marrow derived dendritic cells (BMDCs) (Figure 3C) by flow cytometry. CGP3466b had a minimal effect only at the highest dose.

To determine whether CGP3466b directly impacts T cell activation, we stimulated CD4+ T cells with anti-CD3 and CD28 antibodies in the presence of varying concentrations of drug (Figure 3D). CGP3466b had no effect on interferon-gamma (IFNγ) production or expression of the activation markers CD44 and CD69.

2.4. CGP3466b does not alter CNS immune infiltration in the MOG_{35-55} EAE model

To further examine whether the neuroprotection provided by CGP3466b occurs independent of peripheral anti-inflammatory effects, we quantified the impact of CGP3466b treatment on CNS inflammatory infiltrates. Mice subjected to MOG_{35-55} EAE were treated daily with vehicle or CGP3466b (4 mg/kg) in a prophylactic paradigm (beginning PID 0) and analyses were performed at PID 18 (peak disease) and PID 28. Using immunofluorescence staining of CD45 (expressed by all classes of leukocyte) on PID 18, we detected no difference in the number of infiltrating immune cells in the spinal cord with CGP3466b treatment (Figure 4A). Using the same prophylactic treatment paradigm, we examined the number of Iba1+ microglia/macrophages in the optic nerve at PID 28, but we observed no significant difference (Figure 4B) despite the neuroprotection observed in the same optic nerves *via* SMI-32 staining (Figure 2D). We also examined the impact of CGP3466b on myeloid and lymphoid cell phenotypes in the CNS at peak disease using flow cytometry (Figures 4C–H; Supplementary Figure 3). CGP3466b treatment had no effect on arginase-1 (Arg1) expression in either infiltrating macrophages ($CD11b^+CD45^+Clec12a^+$) (Figure 4C) or microglia ($CD11b^+CD45^+Clec12a^-$) (Figure 4D) within the brain or spinal cord. iNOS, the classical pro-inflammatory macrophage/microglia phenotypic marker, is only expressed at the onset of EAE (41). Consequently, we examined the pro-inflammatory phenotype by examining the effect of CGP3466b on MHC II expression in macrophages (Figure 4E) and microglia (Figure 4F) and found no significant effect. Similarly, we found no significant difference in the proportion of CD4 lymphocytes displaying markers of T helper (Th) 1 ($CD3^+CD4^+IFNγ^+$) (Figure 4G) or Th17 ($CD3^+CD4^+IL\text{-}17^+$) phenotypes (Figure 4H). Together, these results indicate that CGP3466b has minimal effects on the immune response in the MOG_{35-55} EAE model of MS.

3. Discussion

In this study, we evaluated the GAPDH nitrosylation inhibitor CGP3466b as a potential novel therapy for MS. We found that in the MOG_{35-55} EAE model of MS, GAPDH is a major target of nitrosylation within the CNS, which is selectively blocked by systemic treatment with CGP3466b. We further showed that CGP3466b is neuroprotective in the context of neuroinflammation, attenuating disease course in our murine model of MS and reducing axonal damage in the optic nerve. Finally, we showed that CGP3466b has minimal effects on the immune response *in vitro* and *in vivo*, suggesting that CGP3466b is directly neuroprotective and acts independently of the peripheral immune system.

Modest effects of CGP3466b were observed on myeloid cell function only at a high dose (200 nM). Although CGP3466b blocks GAPDH nitrosylation at low nanomolar concentrations (24), at higher concentrations the drug has other targets such as the PCMT1/MST1 signaling pathway (42) and succinate-dependent H_2O_2 release from mitochondrial complex I (43). These lower-affinity targets may explain the observed effects on myeloid cells at high dose. However, it is unlikely that such a high concentration is achieved *in vivo* with the 4 mg/kg dose used in our studies.

There has been longstanding interest in blocking NO-mediated pathways as a means to protect neurons in MS. Microglia, CNS-resident macrophages, and astrocytes – the primary sources of NO – represent a common link in the pathology of relapsing and progressive MS. As previously noted, NO levels increase in active MS lesions and during relapse, leading some to investigate NO as a biomarker (44). Finally, NO directly contributes to neuro-axonal

10.3389/fneur.2022.979659

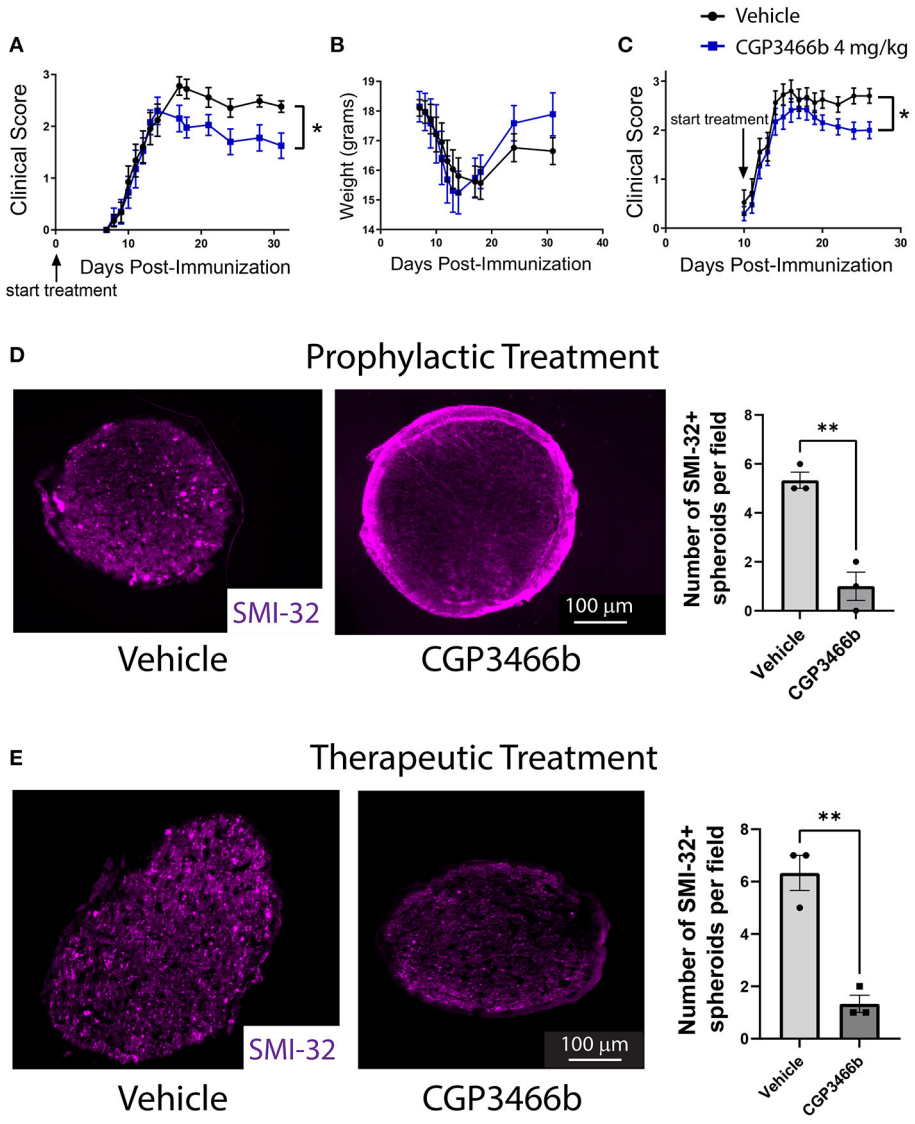

FIGURE 2
Blocking SNO-GAPDH with CGP3466b is neuroprotective in MOG_{35-55} EAE. **(A, B)** CGP3466b 4 mg/kg was administered by daily i.p. injection beginning on post-immunization day 0 (prophylactic paradigm). Clinical scoring was performed by a blinded observer. Prophylactic treatment with CGP3466b attenuated neurologic deficits **(A)** without impacting weight loss **(B)**. Data represent $n = 17$ (vehicle) and $n = 10$ (CGP3466b) mice per group. **(C)** CGP3466b 4 mg/kg was administered by daily i.p. injection beginning on post-immunization day 10 (therapeutic paradigm), and clinical scoring was performed by a blinded observer. Data represent $n = 20$ (vehicle) and $n = 26$ (CGP3466b) mice per group. **(D)** To quantify axonal injury, mice were treated with vehicle or CGP3466b 4 mg/kg by daily i.p. injection beginning on post-immunization day 0, and SMI-32+ axonal spheroids were examined *via* immunofluorescence staining of proximal optic nerve at post-immunization day 28. A representative image is shown (left), along with quantification performed from $n = 3$ mice per group (right). **(E)** Mice were treated with vehicle or CGP3466b 4 mg/kg by daily i.p. injection beginning on post-immunization day 10, and SMI-32+ axonal spheroids were examined *via* immunofluorescence staining of proximal optic nerve at post-immunization day 28. A representative image is shown (*left*), along with quantification performed from $n = 3$ mice per group (*right*). $^*p < 0.05$, $^{**}p < 0.01$ by Mann-Whitney U-test **(A, C)** or student's *t*-test **(D, E)**. Data shown as mean ± SEM.

injury in animal models of neuroinflammation (14). Nonetheless, NO has pleiotropic effects in inflammation, some of which are required for resolution of inflammation or simply for normal function of the nervous system, such that limiting NO production altogether has yielded inconsistent results (45). In contrast, selectively targeting SNO-GAPDH with CGP3466b blocks a specific NO-mediated signaling pathway involved in neuroaxonal injury while preserving other functions of NO.

Interestingly, although treatment with CGP3466b prevented axonal degeneration and mitigated neurologic disability in our model, we did not observe a statistically significant effect of CGP3466b on MBP staining. Although it is possible that our study was underpowered to observe such an effect, it would appear that CGP3466b protects axonal integrity out of proportion to effects on oligodendrocytes. These findings suggest that the pathways producing inflammatory injury differ between neurons and oligodendrocytes. As mentioned above, selective protection of axons by CGP3466b is consistent with previous work demonstrating that reactive oxygen and nitrogen species produce axonal degeneration in EAE independent of myelin injury (14). Although the number of animals analyzed by histological and flow cytometric studies was modest, these experiments were

10.3389/fneur.2022.979659

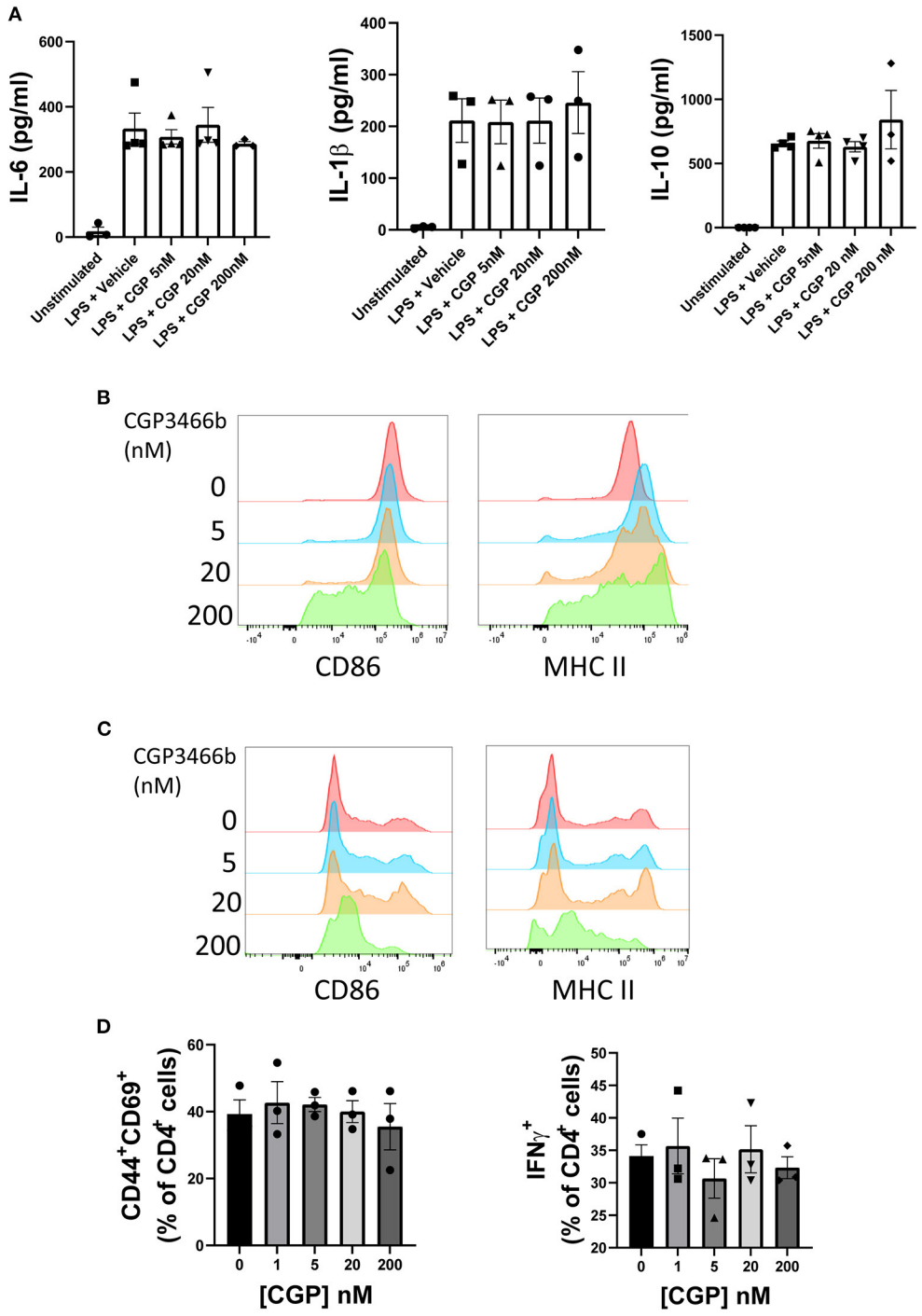

FIGURE 3
CGP3466b has minimal direct effects on myeloid and lymphoid cells *in vitro*. **(A)** Bone marrow derived macrophages (BMMs) were treated with LPS (100 ng/mL) plus vehicle or the indicated concentrations of CGP3466b for 24 h. Cytokine concentrations in media were determined by ELISA. Data represent mean ± SEM of $n = 3$ or $n = 4$ independent experiments performed in triplicate. **(B)** BMMs and **(C)** Bone marrow derived dendritic cells (BMDCs) were treated with LPS (100 ng/mL) plus vehicle or the indicated concentrations of CGP3466b, and expression of activation markers was measured by flow cytometry. Data are a representative example of $n = 3$ independent experiments. **(D)** CD4+ lymphocytes were stimulated with anti-CD3/CD28 antibodies (3 ug/mL) in the presence of vehicle or the indicated concentrations of CGP3466b. Percentage of CD4+ lymphocytes expressing the given activation markers was measured by flow cytometry. Data represent mean ± SEM of three biological replicates.

performed in independent cohorts of mice specifically dedicated to these studies in order to avoid sampling bias. Furthermore, all histological analyses were performed within the same optic nerves, allowing direct comparison of neuroprotective, myelin protective, and immunologic effects of CGP3466b treatment within the same animals.

SNO-GAPDH has been shown to trans-nitrosylate several proteins, including the deacetylating enzyme sirtuin-1 (SIRT1) (20).

10.3389/fneur.2022.979659

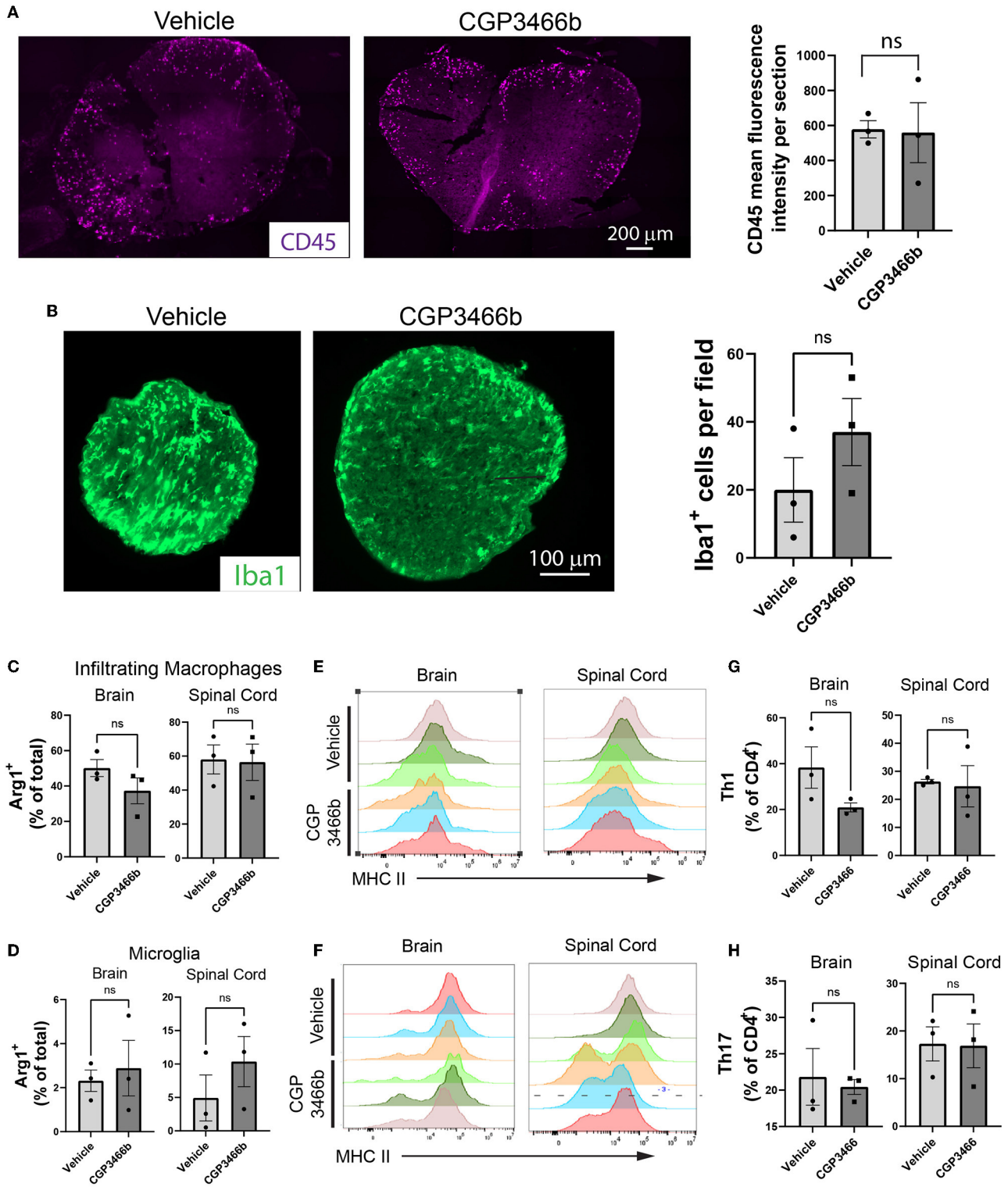

FIGURE 4
CGP3466b does not impact CNS immune infiltration in MOG_{35-55} EAE. **(A)** CD45+ infiltrates in lumbar spinal cord at post-immunization day 18. Mice were treated with vehicle or 4 mg/kg CGP3466b daily starting on post-immunization day 0. A representative image is shown (*left*), along with quantification performed from $n = 3$ mice per group (*right*). **(B)** Iba1+ infiltrates in optic nerve at post-immunization day 28. Mice (the same cohort depicted in Figure 2D) were treated with vehicle or 4 mg/kg CGP3466b daily starting on post-immunization day 0. A representative image is shown (*left*), along with quantification performed from $n = 3$ mice per group (*right*). **(C)** Infiltrating macrophages and **(D)** resident microglia in the brain and spinal cord were examined via flow cytometry on post-immunization day 18 for expression of arginase-1 as a percentage of total macrophages or microglia, respectively. Data represent mean ± SEM of 3 mice per group. **(E)** Infiltrating macrophages and **(F)** resident microglia were examined *via* flow cytometry on post-immunization day 18 for expression of MHC II, shown as mean fluorescence intensity. Data shown from 3 mice per group. **(G)** Th1 cells and **(H)** Th17 cells were quantified *via* flow cytometry on post-immunization day 18 in the brain and spinal cord as a percentage of total CD4+ cells. Data represent mean ± SEM of 3 mice per group. All statistical analyses performed with student's *t*-test.

TABLE 1 Antibodies.

Antibody, conjugate	Clone	Company
CD4, eFluor450	RM4-5	Invitrogen
CD3, PerCP/Cy5.5	145-2C11	Biolegend
CD45, BV605	30-F11	Biolegend
IL-12, APC	C15.6	Biolegend
IL-17, APC	ebio17b7	Invitrogen
Arg1, PE-Cy7	A1exF5	Invitrogen
Ly6G, BV785	1A8	Biolegend
Clec12a, APC	5D3	Biolegend
CD11b, BV510	M1/70	Biolegend
CD11c, PE	N418	Biolegend
F4/80, APC/Fire 750	BM8	Biolegend
Neurofilament H (NF-H), purified	SMI 32	Biolegend
Class II, PerCP	M5/114.15.2	Biolegend
CD44, PE-Cy7	IM8	Biolegend
CD69, BV650	30-F11	Biolegend
GAPDH	6C5	Millipore sigma
β-tubulin	AA2	Millipore sigma
Iba-1	NB100-1028	NovusBio
Myelin basic protein	82–87	Millipore
CD45, APC	30-F11	Biolegend

SIRT1 is a key regulator of mitochondrial biogenesis (46, 47), and SNO-GAPDH has also been shown to trans-nitrosylate several mitochondrial enzymes (48). Therefore, it is possible that blocking CGP3466b is protective in neurons and axons because it prevents SNO-GAPDH-mediated mitochondrial dysfunction. Future studies will examine the effect of CGP3466b on mitochondria health in neurons, along with other potential mechanisms underlying its neuroprotection.

Because CGP3466b has been evaluated in Phase II clinical trials, there is an established safety profile and low threshold for clinical translation. Although CGP3466b did not have a significant effect on the clinical course of Parkinson's disease in humans, this is likely because Parkinson's disease pathology is complex with much less dependence on oxidative/nitrosative stress than the MPTP mouse model in which CGP3466b showed benefit. In contrast, MS is a primary inflammatory disease in which macrophage/microglia and astrocyte generation of NO is a known aspect of pathology in both the human disease and the EAE mouse model. As such, the rationale for involvement of SNO-GAPDH in human disease is much stronger in the case of MS.

All disease modifying therapies currently approved for MS act by targeting the immune system – primarily by limiting peripheral immune activation or preventing peripheral immune cells from infiltrating the CNS (49). However, none of these medications limit CNS damage during a relapse or, most importantly, slow disability accrual in non-active progressive MS, largely because progressive MS pathology is driven by compartmentalized innate immune activation instead of the T-cell driven attack seen in relapsing-remitting MS (7, 50). Therefore, neuroprotective therapies that prevent inflammatory CNS injury represent a major goal in MS research, regardless of the source or stage of inflammation. Such therapies might be used as adjunct treatments in combination with immunomodulatory therapies in relapsing MS and/or as first-in-class agents to slow neurodegeneration and therefore disability accrual in progressive MS. Future studies will evaluate CGP3466b as an adjunct therapy in murine models of MS.

In summary, our data indicate that blocking GAPDH nitrosylation with CGP3466b significantly attenuates disability in the murine EAE model of MS through a neuroprotective mechanism independent of the peripheral immune system. Given the substantial need for neuroprotective agents as adjunct therapies in both relapsing and progressive MS and due to its established safety profile, CGP3466b holds promise as a therapeutic strategy in MS that merits further investigation.

3.1. Materials and methods

3.1.1. Mice

Wild-type C57BL/6J mice were purchased from the Jackson Laboratory (stock # 000664) and housed in a dedicated Johns Hopkins rodent facility with regulated temperature (20-22°C), 50% humidity, and a 12-hour light/12-hour dark cycle with free access to water and solid food. Protocols were approved by the Johns Hopkins Institutional Animal Care and Use Committee (Protocol MO21M370).

3.1.2. Antibodies

A list of antibodies used in the reported experiments is included in Table 1.

3.1.3. EAE induction and scoring

Active EAE was induced in female C57BL/6J mice (8–12-week-old) after 1-week acclimatization to the animal facility. MOG_{35-55} peptide dissolved in PBS at a concentration of 2 mg/mL was mixed 1:1 with complete Freund's adjuvant (8 mg/ml Tuberculin toxin in incomplete Freund's adjuvant), then mixed for 10 min into an emulsion. On day 0, mice were immunized by injecting 50 μl of the emulsion subcutaneously into each of two sites on the lateral abdomen. In addition, on day 0 and again on day 2, mice were injected intraperitoneally with 250 ng pertussis toxin. Control animals were treated with complete Freund's adjuvant and pertussis toxin alone. Scoring was performed in a blinded manner according to the following scale: 0, no clinical deficit; 0.5, partial loss of tail tone; 1.0, complete tail paralysis or both partial loss of tail tone plus awkward gait; 1.5, complete tail paralysis and awkward gait; 2.0, tail paralysis with hind limb weakness evidenced by foot dropping between bars of cage lid while walking; 2.5, hind limb paralysis with little to no weight-bearing on hind limbs (dragging), but with some movement possible in legs; 3.0, complete hind limb paralysis with no movement in lower limbs; 3.5, hind limb paralysis with some weakness in forelimbs; 4.0, complete tetraplegia but with some movement of head; 4.5, moribund; and 5.0, dead.

3.1.4. Treatment of mice with CGP3466b

CGP3466b maleate (Tocris, cat # 2966) stock solution (50 mM in DMSO) was diluted to 4% DMSO in PBS as a working solution (final CGP3466b concentration 20–800 μg/ml depending on dosage to be delivered). Mice were treated daily with i.p. injection of drug or an equal volume of vehicle control (4% DMSO in PBS). Treatment either began on the same day as immunization with MOG_{35-55} (PID 0) or on PID 10.

3.1.5. Biotin switch assay

The assay was performed as previously described with slight modifications (34). Briefly, spinal cords were flushed from the spinal column with hydrostatic pressure and then then dissolved in RIPA/HEN (HEN buffer adjusted to contain 1% Triton X-100, 1% sodium deoxycholate, 0.1% SDS) with a hand-held tissue homogenizer. The homogenate was clarified by spinning at 13,000 g for 10 min at 4°C. Supernatant was collected and stored at −80°C until use. Free thiol groups were blocked with 20 mM MMTS (methyl methanethiosulfonate) for 20 min. Protein was precipitated in acetone and then resuspended in a labeling solution containing 50 mM sodium ascorbate and 0.8 mM biotin-HPDP for 1 h. Protein was precipitated in ice-cold acetone, resuspended, and pulled-down overnight with high-capacity neutravidin agarose beads. The beads were washed and biotinylated proteins were eluted with HEN/10 buffer (HEN buffer diluted 1/10 in water) containing 1% beta-mercaptoethanol (Sigma). Protein was resolved by SDS/PAGE. Bands were transferred to PVDF Immobilon P membranes using a wet transfer, blocked in TBS-T containing 5% milk, and probed overnight at 4°C with primary antibodies. Blots were then washed and stained with HRP-conjugated secondary antibody (Jackson ImmunoResearch). Immunoblots were visualized using the SuperSignal West ECL system (ThermoFisher) followed by film exposure. Bands were quantified with ImageJ software. To correct for differences in sample loading, a ratio of SNO-GAPDH to total GAPDH band intensity was calculated, and values were normalized to the CFA alone control group.

3.1.6. Immunofluorescence imaging

Mice were euthanized by overdose of isoflurane (adjusting the isoflurane flow rate to 5% until breathing stopped) and then perfused *via* cardiac puncture with ice-cold PBS followed by a paraformaldehyde perfusion. After perfusion, optic nerves and spinal cords were dissected out. Tissue was fixed in paraformaldehyde overnight, sucrose protected with 30% sucrose, and frozen in OCT. Cryosections (12 μm) from proximal optic nerve were incubated with anti-SMI-32, anti-Iba1, or anti-MBP antibodies overnight, washed with PBS-T, and incubated with anti-mouse secondary antibody. Spinal cord sections (12 μm) were incubated with anti-CD45 (APC conjugated) antibody overnight at 4°C. Sections were imaged on a Zeiss Axio Observer Z1 epifluorescence microscope and Zeiss 710 confocal microscope with the appropriate excitation and emission filters. SMI-32 and Iba-1 staining was quantified by automated counting of discrete particles that were determined to be a positive signal. MBP staining was quantified by masking the MBP+ regions of the optic nerve and calculating the MBP- regions, then dividing to yield a %MBP calculation. Staining for SMI-32, Iba1, and MBP was performed from the same optic nerves in order to compare neuroprotection with macrophage/microglia activation and demyelination in the same mice. All quantification was performed with ImageJ software.

3.1.7. Isolation, culture, and treatment of murine bone marrow derived dendritic cells (BMDCs) and bone marrow derived macrophages (BMMs)

Cells were isolated as described (51). Briefly, femurs were removed from 6 to 10-wk-old C57BL/6J mice, cut on both ends, and marrow was flushed with PBS. Bone marrow cells were then pelleted at 1,500 rpm, resuspended in red blood cell lysis buffer, and after 1 min the reaction was quenched with excess PBS. After another centrifugation, cells were resuspended in complete RPMI media consisting of RPMI-1640 with GlutaMAX supplement, along with 10% FBS, 1% penicillin-streptomycin, and 50 μM beta-mercaptoethanol (Sigma). On day 0, ~2×10^6 cells were then seeded per 100-mm plate in 10 mL media containing 20 ng/mL recombinant murine M-CSF (Peprotech). On day 3, an additional 10 mL fresh cRPMI media containing 20 ng/mL M-CSF was added to each plate. On day 5, half the culture supernatant from each plate was removed and centrifuged, and the pelleted cells resuspended in 10 mL fresh cRPMI with 20 ng/mL M-CSF and added back to the plates. On day 8, all non-adherent cells (representing the BMDC fraction) were collected, pelleted by centrifugation, resuspended in fresh cRPMI media with 20 ng/mL GM-CSF, and plated into 96-well dishes. These BMDCs were then treated overnight with or without LPS (Sigma) 100 ng/ml plus the indicated doses of CGP3466b (dissolved in DMSO) or vehicle (DMSO alone). The following day (day 9), these cells were then assayed by flow cytometry. Adherent macrophages (BMMs) were removed from the petri dish with macrophage detachment solution (Promocell) and replated into 6 well-plates along with LPS 100 ng/mL and the indicated doses of CGP3466b or vehicle. These cells were then assayed by flow cytometry or cytokine ELISA.

3.1.8. Preparation of tissue for flow cytometry

Mice were euthanized by overdose of isoflurane (adjusting the isoflurane flow rate to 5% until breathing stopped) then perfused with ice-cold PBS *via* cardiac puncture. Brain and spinal cord were collected, mechanically dissociated, then chemically dissociated with collagenase (200 U/mL) and DNase (100 U/mL) with constant shaking for 20 min. Cells were then passed through a 100 μM filter and washed with PBS. Myelin debris was removed by resuspending the cell pellet with a debris removal solution (Miltenyi Biotec), overlaying with PBS, and spinning at 3,000 g, then removing the myelin debris layer. Cell pellets were then resuspended in PBS, passed through a 100 μM filter, and stained with antibody as described below.

3.1.9. CD4+ T-cell isolation and culture

T-cells were isolated by generating single-cell suspensions from the spleen and lymph nodes of 6–10-week-old C57BL/6 mice. Spleens were disrupted with the plunger of a syringe over a 70-μm nylon cell strainer (BD Falcon), then cells were pelleted by centrifugation (500 × g for 5 min) and resuspended in fresh FACS buffer. CD4+ cells were then isolated by negative selection using the Mojo CD4+ cell isolation kit from Biolegend (Catalog 48006) according to the manufacturer's instructions. Plates were coated overnight at 4°C with

anti-mouse CD3 antibody (3 μg/mL). T cells were resuspended in complete RPMI (RPMI plus 10%FBS, 1% Pen-strep, 1% glutamax, 0.1% 2-mercaptoethanol) along with 3 ug/mL anti-mouse CD28 antibody. Cells were cultured for 96 h and treated for the last 24 h with vehicle or CGP3466b before proceeding with flow cytometry staining.

3.1.10. ELISA

After overnight stimulation with LPS 100 ng/mL ± CGP3466b or vehicle, BMM culture supernatants were collected and cytokine production was assayed using ELISA kits for IL-1β, IL-6, and IL-10 purchased from eBioscience, according to manufacturer's instructions. Plates were read at 450 nm on a tabletop colorimetric spectrophotometer.

3.1.11. Flow cytometry staining

For panels involving T cells, cells were first resuspended in a solution of complete RPMI with brefeldin/Monensin and PMA/ionomycin. BMDCs and BMMs were treated with brefeldin and monensin. These treatments lasted 4 h at 37°C.

All staining was performed in the dark at room temperature. Cells were first stained with zombie NIR (1:1,000) for 10 min along with CD16/32 (1:200) dissolved in PBS. Cells were then washed and resuspended in a solution of PBS+2% FBS+1 mm EDTA and stained with the relevant antibodies. All surface antibodies were stained at a 1:300 dilution. Cells were then washed and incubated in FoxP3 fixation/permeabilization buffer following the manufacturer recommended protocol. Intracellular staining was performed with conjugated antibodies (1:200) against the specified proteins in permeabilization buffer for 1 h, washed twice, and then analyzed cells with a Cytek Aurora Flow cytometer. Data analysis was performed with FlowJo software.

3.1.12. Statistical analyses

All statistical analyses were performed using GraphPad Prism software. Details of statistical analyses for each experiment can be found in the figures and figure legends.

Data availability statement

The original contributions presented in the study are included in the article/Supplementary material, further inquiries can be directed to the corresponding author.

Ethics statement

The animal study was reviewed and approved by Johns Hopkins Institutional Animal Care and Use Committee.

Author contributions

WG contributed to project and experimental design, data acquisition, data analysis/interpretation, and drafting of the manuscript and figures. SH, KC, SS, PG, and EA contributed to data acquisition. MK contributed to project and experimental design, data acquisition, data analysis/interpretation, drafting/editing of the manuscript and figures, and provided funding support. All authors contributed to the article and approved the submitted version.

Funding

This work was supported by NIH/NINDS Grant K08NS104266 and Conrad N. Hilton Foundation Marilyn Hilton Bridging Award for Physician Scientists Grant 17316 to MK. WG was supported by NIH MSTP Grant T32 GM136577 and the American Association of Immunologists' Careers in Immunology Fellowship Program.

Acknowledgments

The authors would like to thank Matthew Smith, Bindu Paul, Judy Lee, Michelle Taylor, Thomas Garton, and Em Harrington for technical assistance.

Conflict of interest

MK has received consulting fees from Biogen Idec, Genentech, Janssen Pharmaceuticals, Novartis, OptumRx, and TG Therapeutics on topics unrelated to this manuscript.

The remaining authors declare that the research was conducted in the absence of any commercial or financial relationships that could be construed as a potential conflict of interest.

Publisher's note

Supplementary material

The Supplementary Material for this article can be found online at: https://www.frontiersin.org/articles/10.3389/fneur.2022.979659/full#supplementary-material

References

1. Wallin MT, Culpepper WJ, Campbell JD, Nelson LM, Langer-Gould A, Marrie RA, et al. The prevalence of MS in the United States. *Neurology.* (2019) 92:e1029–40. doi: 10.1212/WNL.0000000000007035

2. Reich DS, Lucchinetti CF, Calabresi PA. (2018). *Multiple Sclerosis.* (1483) 169–80. doi: 10.1056/NEJMra1401483

3. Friese MA, Schattling B, Fugger L. Mechanisms of neurodegeneration and axonal dysfunction in multiple sclerosis. *Nature Rev Neurol.* (2014) 10:225–38. doi: 10.1038/nrneurol.2014.37

4. Chitnis T, Weiner HL. CNS inflammation and neurodegeneration. *J Clin Invest.* (2017) 127:3577–87. doi: 10.1172/JCI90609

5. Frischer JM, Bramow S, Dal-Bianco A, Lucchinetti CF, Rauschka H, Schmidbauer M, et al. The relation between inflammation and neurodegeneration in multiple sclerosis brains. *Brain*. (2009) 132:1175. doi: 10.1093/brain/awp070

6. Grigoriadis N, van Pesch V. A basic overview of multiple sclerosis immunopathology. *Eu J Neurol*. (2015) 22 Suppl 2:3–13. doi: 10.1111/ene.12798

7. Lassmann H, van Horssen J, Mahad D. Progressive multiple sclerosis: Pathology and pathogenesis. In *Nature Reviews Neurology*. Nature Publishing Group. (2012). (Vol. 8, Issue 11, 647–656.). doi: 10.1038/nrneurol.2012.168

8. Mahad DH, Trapp BD, Lassmann H. Pathological mechanisms in progressive multiple sclerosis. *Lancet Neurol*. (2015) 14:183–93. doi: 10.1016/S1474-4422(14)70256-X

9. Wei W, Ma D, Li L, Zhang L. Progress in the application of drugs for the treatment of multiple sclerosis. *Front Pharmacol*. (2021) 12:724718. doi: 10.3389/FPHAR.2021.724718

10. Biswas S, Das R, Banerjee ER, Biswas S, Das R, Banerjee ER, et al. Role of free radicals in human inflammatory diseases. *AIMS Biophysics*. (2017) 4:596. doi: 10.3934/biophy.2017.4.596

11. Sharma JN, Al-Omran A, Parvathy SS. Role of nitric oxide in inflammatory diseases. *Inflammopharmacology*. (2007) 15:252–9. doi: 10.1007/s10787-007-0013-x

12. Bö L, Dawson TM, Wesselingh S, Möurk S, Choi S, Kong PA, et al. Induction of nitric oxide synthase in demyelinating regions of multiple sclerosis brains. *Ann Neurol*. (1994) 36:778–86. doi: 10.1002/ana.410360515

13. Smith KJ, Lassmann H. The role of nitric oxide in multiple sclerosis. *Lancet Neurol*. (2002) 1:232–41. doi: 10.1016/S1474-4422(02)00102-3

14. Nikić I, Merkler D, Sorbara C, Brinkoetter M, Kreutzfeldt M, Bareyre FM, et al. A reversible form of axon damage in experimental autoimmune encephalomyelitis and multiple sclerosis. *Nat Med*. (2011) 17:495–9. doi: 10.1038/nm.2324

15. Smith KJ, Kapoor R, Hall SM, Davies M. Electrically active axons degenerate when exposed to nitric oxide. *Ann Neurol*. (2001) 49:470–6. doi: 10.1002/ana.96

16. Hess DT, Matsumoto A, Kim SO, Marshall HE, Stamler JS. Protein S-nitrosylation: purview and parameters. *Nat Rev Mol Cell Biol*. (2005) 6:150–66. doi: 10.1038/nrm1569

17. Kovacs I, Lindermayr C. Nitric oxide-based protein modification: formation and site-specificity of protein S-nitrosylation. *Front Plant Sci*. (2013) 4:137. doi: 10.3389/fpls.2013.00137

18. Hara MR, Agrawal N, Kim SF, Cascio MB, Fujimuro M, Ozeki Y, et al. S-nitrosylated GAPDH initiates apoptotic cell death by nuclear translocation following Siah1 binding. *Nat Cell Biol*. (2005) 7:665–74. doi: 10.1038/ncb1268

19. Sen N, Hara MR, Kornberg MD, Cascio MB, Bae BI, Shahani N, et al. Nitric oxide-induced nuclear GAPDH activates p300/CBP and mediates apoptosis. *Nat Cell Biol*. (2008) 10:866. doi: 10.1038/ncb1747

20. Kornberg MD, Sen N, Hara MR, Juluri KR, Nguyen JVK, Snowman AM, et al. GAPDH mediates nitrosylation of nuclear proteins. *Nat Cell Biol*. (2010) 12:1094. doi: 10.1038/ncb2114

21. Bizzozero OA, Zheng J. Identification of major s-nitrosylated proteins in murine experimental autoimmune encephalomyelitis. *J Neurosci Res*. (2009) 87:2881. doi: 10.1002/jnr.22113

22. Harraz MM, Snyder SH. Nitric oxide-GAPDH transcriptional signaling mediates behavioral actions of cocaine. *CNS Neurol Disord Drug Targets*. (2015) 14:757. doi: 10.2174/1871527314666150529150143

23. Waldmeier PC, Boulton AA, Cools AR, Kato AC, Tatton WG. Neurorescuing effects of the GAPDH ligand CGP 3466B. *J Neural Trans Suppl*. (2000) 60:197–214. doi: 10.1007/978-3-7091-6301-6_13

24. Hara MR, Thomas B, Cascio MB, Bae BI, Hester LD, Dawson VL, et al. Neuroprotection by pharmacologic blockade of the GAPDH death cascade. *Proceed Nat Acad Sci USA*. (2006) 103:3887–9. doi: 10.1073/pnas.0511321103

25. Kragten E, Lalande I, Zimmermann K, Roggo S, Schindler P, Müller D, et al. Glyceraldehyde-3-phosphate dehydrogenase, the putative target of the antiapoptotic compounds CGP 3466 and R-(-)-deprenyl. *J Biol Chem*. (1998) 273:5821–8. doi: 10.1074/jbc.273.10.5821

26. Miller R, Bradley W, Cudkowicz M, Hubble J, Meininger V, Mitsumoto H, et al. Phase II/III randomized trial of TCH346 in patients with ALS. *Neurology*. (2007) 69:776–84. doi: 10.1212/01.wnl.0000269676.07319.09

27. Olanow CW, Schapira AH, LeWitt PA, Kieburtz K, Sauer D, Olivieri G, et al. TCH346 as a neuroprotective drug in Parkinson's disease: a double-blind, randomised, controlled trial. *Lancet Neurol*. (2006) 5:1013–20. doi: 10.1016/S1474-4422(06)70602-0

28. Konnova EA, Swanberg M. Animal models of Parkinson's disease. *Parkinson's Dis Pathogen Clin Aspects*. (2018) 83–106. doi: 10.15586/codonpublications.parkinsonsdisease.2018.ch5

29. Sorenson EJ. Transgenic animal models of amyotrophic lateral sclerosis. *Peripheral Neuropathy*. (2005) 2:1585–93. doi: 10.1016/B978-0-7216-9491-7.50069-7

30. Parkinson JF, Mitrovic B, Merrill JE. The role of nitric oxide in multiple sclerosis. *J Mol Med*. (1997) 75:174–86. doi: 10.1007/s001090050102

31. Procaccini C, Rosa de, Pucino V, Formisano VL, Matarese G. Animal models of multiple sclerosis. *Eu J Pharmacol*. (2015) 759:182. doi: 10.1016/j.ejphar.2015.03.042

32. Constantinescu CS, Farooqi N, O'Brien K, Gran B. Experimental autoimmune encephalomyelitis (EAE) as a model for multiple sclerosis (MS). *Br J Pharmacol*. (2011) 164:1079. doi: 10.1111/j.1476-5381.2011.01302.x

33. Robinson AP, Harp CT, Noronha A, Miller SD. The experimental autoimmune encephalomyelitis (EAE) model of MS: utility for understanding disease pathophysiology and treatment. *Handb Clin Neurol*. (2014) 122:173–89. doi: 10.1016/B978-0-444-52001-2.00008-X

34. Jaffrey SR, Snyder SH. The biotin switch method for the detection of S-nitrosylated proteins. *Sci STKE Signal Transduct Know Environ*. (2001) 2001:L1. doi: 10.1126/scisignal.862001pl1

35. Xu R, Serritella AV, Sen T, Farook JM, Sedlak TW, Baraban J, et al. Behavioral effects of cocaine mediated by nitric oxide-GAPDH transcriptional signaling. *Neuron*. (2013) 78:623–30. doi: 10.1016/j.neuron.2013.03.021

36. Sen N, Hara MR, Ahmad AS, Cascio MB, Kamiya A, Ehmsen JT, et al. GOSPEL: a neuroprotective protein that binds to GAPDH upon S-nitrsoylation. *Neuron*. (2009) 63:81–91. doi: 10.1016/j.neuron.2009.05.024

37. Guha P, Harraz MM, Snyder SH. Cocaine elicits autophagic cytotoxicity via a nitric oxide-GAPDH signaling cascade. *Proc Natl Acad Sci U S A*. (2016) 113:1417–22. doi: 10.1073/pnas.1524860113

38. Kezuka T, Usui Y, Goto H. Analysis of the pathogenesis of experimental autoimmune optic neuritis. *J Biomed Biotechnol*. (2011) 2011:4046. doi: 10.1155/2011/294046

39. Sättler MB, Togni M, Gadjanski I, Sühs KW, Meyer N, Bähr M, et al. Strain-specific susceptibility for neurodegeneration in a rat model of autoimmune optic neuritis. *J Neuroimmunol*. (2008) 77–86. doi: 10.1016/j.jneuroim.2007.10.021

40. Gharagozloo M, Smith MD, Jin J, Garton T, Taylor M, Chao A, et al. Complement component 3 from astrocytes mediates retinal ganglion cell loss during neuroinflammation. *Acta Neuropathol*. (2021) 142:899–915. doi: 10.1007/s00401-021-02366-4

41. Giles DA, Washnock-Schmid JM, Duncker PC, Dahlawi S, Ponath G, Pitt D, et al. Myeloid cell plasticity in the evolution of central nervous system autoimmunity. *Ann Neurol*. (2018) 83:131–41. doi: 10.1002/ana.25128

42. Liang F, Shi L, Zheng J, Chen S, Wang Y, Zhang J, et al. Neuroprotective Effects of CGP3466B on apoptosis are modulated by protein-L-isoaspartate (D-aspartate) O-methyltransferase/Mst1 pathways after traumatic brain injury in rats. *Scien Rep*. (2017) 7:1–8. doi: 10.1038/s41598-017-08196-3

43. Zoccarato F, Cappellotto M, Alexandre A. Clorgyline and other propargylamine derivatives as inhibitors of succinate-dependent H(2)O(2) release at NADH:UBIQUINONE oxidoreductase (Complex I) in brain mitochondria. *J Bioenerg Biomembr*. (2008) 40:289–96. doi: 10.1007/s10863-008-9160-z

44. Abdel Naseer M, Rabah AM, Rashed LA, Hassan A, Fouad AM. Glutamate and nitric oxide as biomarkers for disease activity in patients with multiple sclerosis. *Multi Sclero Relat Disord*. (2020) 38:1873. doi: 10.1016/j.msard.2019.101873

45. Encinas JM, Manganas L, Enikolopov G. Nitric oxide and multiple sclerosis. *Curr Neurol Neurosci Rep*. (2005) 5:232–8. doi: 10.1007/s11910-005-0051-y

46. Chuang YC, Chen SD, Jou SB, Lin TK, Chen SF, Chen NC, et al. Sirtuin 1 regulates mitochondrial biogenesis and provides an endogenous neuroprotective mechanism against seizure-induced neuronal cell death in the hippocampus following status epilepticus. *Int J Mol Sci*. (2019) 20:3588. doi: 10.3390/ijms20143588

47. Majeed Y, Halabi N, Madani AY, Engelke R, Bhagwat AM, Abdesselem H, et al. SIRT1 promotes lipid metabolism and mitochondrial biogenesis in adipocytes and coordinates adipogenesis by targeting key enzymatic pathways. *Scien Rep*. (2021) 11:1–19. doi: 10.1038/s41598-021-87759-x

48. Kohr MJ, Murphy E, Steenbergen C. Glyceraldehyde-3-phosphate dehydrogenase acts as a mitochondrial trans-S-nitrosylase in the heart. *PLoS ONE*. (2014) 9:e111448. doi: 10.1371/journal.pone.0111448

49. Callegari I, Derfuss T, Galli E. Update on treatment in multiple sclerosis. *La Presse Médicale*. (2021) 50:104068. doi: 10.1016/j.lpm.2021.104068

50. Rice CM, Cottrell D, Wilkins A, Scolding NJ. Primary progressive multiple sclerosis: Progress and challenges. *J Neurol Neurosurg Psychiatry*. (2013) 84:1100–6. doi: 10.1136/jnnp-2012-304140

51. Lutz MB, Kukutsch N, Ogilvie ALJ, Rößner S, Koch F, Romani N, et al. An advanced culture method for generating large quantities of highly pure dendritic cells from mouse bone marrow. *J Immunol Methods*. (1999) 223:77–92. doi: 10.1016/S0022-1759(98)00204-X